Materials Today Bio 29 (2024) 101370

Contents lists available at ScienceDirect

Materials Today Bio

journal homepage: www.journals.elsevier.com/materials-today-bio

Scalable fabrication of freely shapable 3D hierarchical Cu-doped hydroxyapatite scaffolds via rapid gelation for enhanced bone repair

Hui Yang [a,b,*,1], Sirui Huang [b,c,1], Xinwei Zhu [b,1], Yasi Chen [a,b], Chunming Xu [b,d], Ruohan Li [e], Pan Bu [f], Yufan Jiang [e], Changwei Li [a], Jie Yang [a], Zhenyi Chen [a], Weijie Peng [b,**], Lin Liu [b,d,***]

[a] School of Medical and Information Engineering, Gannan Medical University, Ganzhou 341000, China
[b] Jiangxi Provincial Key Laboratory of Tissue Engineering, Gannan Medical University, Ganzhou 341000, China
[c] School of Public Health and Health Management, Gannan Medical University, Ganzhou 341000, China
[d] School of Basic Medicine, Gannan Medical University, Ganzhou 341000, China
[e] Third Clinical College, Gannan Medical University, Ganzhou, 341000, China
[f] School of Rehabilitation Medicine, Gannan Medical University, Ganzhou 341000, China

ARTICLE INFO

Keywords:
Bioceramics
Porous scaffold
Rapid gelation
Bone repair

ABSTRACT

Critical-sized bone defects present a formidable challenge in tissue engineering, necessitating innovative approaches that integrate osteogenesis and angiogenesis for effective repair. Inspired by the hierarchical porous structure of natural bone, this study introduces a novel method for the scalable production of ultra-long, copper-doped hydroxyapatite (Cu-HAp) fibers, utilizing the rapid gelation properties of guar gum (GG) under controlled conditions. These fibers serve as foundational units to fabricate three-dimensional porous scaffolds with a biomimetic hierarchical architecture. The scaffolds exhibit a broad pore size distribution (1–500 μm) and abundant nanoporous features, mimicking the native bone extracellular matrix. Physicochemical characterization and *in vitro* assays demonstrated that the copper doping significantly enhanced osteogenic and angiogenic activities, with optimized concentrations (0.8 % and 1.2 % Cu) facilitating the upregulation of osteogenesis-related genes and proteins, as well as promoting endothelial cell proliferation. *In vivo* studies further confirmed the scaffolds' efficacy, with the 1.2Cu-HAp group showing a remarkable increase in bone regeneration (bone volume/total volume ratio: 35.7 ± 1.87 %) within the defect site. This research offers a promising strategy for the rapid fabrication of multifunctional scaffolds that not only support bone tissue repair but also actively accelerate the healing process through enhanced vascularization.

1. Introduction

Despite significant advances in bone tissue engineering, the challenge of repairing critical-sized bone defects remains unresolved [1]. Bone repair is a complex biological process that is regulated by a combination of chemical stimuli from the microenvironment and physical factors, such as the structure of the extracellular matrix [2,3]. Numerous studies have shown that angiogenesis—the formation of new blood vessels—is a crucial early step in bone repair. Angiogenesis not only supplies the necessary nutrients and oxygen for bone regeneration but also creates a favorable microenvironment for the interaction of osteoblasts and osteoclasts [4]. Thus, constructing an optimal bone tissue engineering system that can rapidly induce neovascularization within the bone defect area, thereby accelerating the bone repair process, remains a pressing challenge.

HAp, a natural mineral component of bone tissue, is recognized for its excellent biocompatibility, bioactivity, and osteoconductivity, making it a promising candidate for bone repair materials [5]. However, pure HAp materials have limited potential to promote angiogenesis. To address this, many studies have explored loading growth factors such as

* Corresponding author. School of Medical and Information Engineering, Gannan Medical University, Ganzhou 341000, China.
** Corresponding author.
*** Corresponding author. Jiangxi Provincial Key Laboratory of Tissue Engineering, Gannan Medical University, Ganzhou 341000, China.
E-mail addresses: yanghui_2521@163.com (H. Yang), pengweijie@gmu.edu.cn (W. Peng), liulin467@gmu.edu.cn (L. Liu).
[1] These authors contributed equally to this work.

https://doi.org/10.1016/j.mtbio.2024.101370
Received 9 September 2024; Received in revised form 17 November 2024; Accepted 25 November 2024
Available online 27 November 2024
2590-0064/© 2024 The Authors. Published by Elsevier Ltd. This is an open access article under the CC BY-NC license (http://creativecommons.org/licenses/by-nc/4.0/).

vascular endothelial growth factor (VEGF) onto HAp scaffolds to enhance their angiogenic properties [6,7]. Yet, these approaches are hampered by challenges such as maintaining growth factor activity and achieving controlled, sustained release [8]. Research has also identified that trace elements—like zinc, magnesium, silicon, manganese, and copper—play significant roles in modulating cellular behavior, mineralization, and angiogenesis during bone formation [9]. Among these, copper ions have been particularly noted for their critical role in promoting angiogenesis and stimulating vascular endothelial cell formation [10]. By incorporating copper ions into HAp materials, it is possible not only to accelerate angiogenesis but also to achieve sustained copper ion release within the material [11]. This sustained release creates a mild and persistent chemical stimulation within the microenvironment, thereby ensuring effective bone tissue repair.

Cancellous bone is a highly porous, three-dimensionally interconnected tissue with irregular and complex pore shapes, ranging from 10 to 600 μm in size. This unique pore distribution allows the bone to maintain structural strength while remaining lightweight [12]. Studies have shown that the pore structure of the extracellular matrix is a key factor in regulating the rapid repair of bone tissue [13]. Large pores (>200 μm) facilitate bone mineral deposition and new bone formation, while smaller pores (<200 μm) support cell adhesion, migration, and angiogenesis [14]. Micropores (<50 μm) are also crucial for immune regulation, which is closely linked to osteogenesis [15]. In nature, silkworm cocoons are formed from ultra-long silk fibroin fibers that are tightly wound in a layered and disordered manner, creating a highly porous, three-dimensional network. This structure, with its irregular and multiscale pores, supports ventilation and water exchange, resembling the porous structure of cancellous bone [16]. Furthermore, the disordered fiber structure provides high flexibility and elasticity, allowing for localized deformation under external forces while maintaining overall structural integrity [17,18]. Inspired by these principles, we hypothesize that using a single ultra-long fiber as a structural unit could enable the construction of bone-like scaffolds with hierarchical pore sizes and interconnected porosity. Additionally, the inherent brittleness of ceramic materials necessitates the use of ceramic/polymer composite precursors (such as composite gels) to effectively achieve three-dimensional fiber winding and assembly, resulting in a three-dimensionally interconnected bone-like tissue structure.

Building on this concept, our research successfully developed a method for the mass production of ultra-long, continuous copper-doped HAp/guar gum (GG) gel fibers by leveraging the strong affinity between GG and copper ions in an alkaline environment. These gel fibers exhibit excellent transferability and moldability, and they were used as structural units to construct copper-doped hydroxyapatite (HAp) fiber scaffolds with biomimetic hierarchical pore structures. The hierarchical pore architecture of the scaffold, combined with the chemical stimulation provided by the sustained release of copper ions, is anticipated to significantly enhance the bone repair process. Consequently, we systematically evaluated the physicochemical properties, as well as the osteogenic and angiogenic activities, of the porous scaffolds. The results indicate that moderate copper doping significantly enhances bone repair, offering a novel approach for the rapid fabrication of functional hierarchical HAp porous scaffolds.

2. Experimental section

2.1. Preparation of Cu-HAp porous scaffold

The fabrication of copper-doped hydroxyapatite (Cu-HAp) porous scaffolds was achieved through a rapid gelation process. All chemicals procured from Aladdin Corp. were utilized without additional purification. The synthesis procedure encompassed the following sequential steps: Initially, 4.61 g of $Ca(NO_3)_2{\cdot}4H_2O$, 0.038 g of $Cu(NO_3)_2{\cdot}3H_2O$, and 0.5 g of GG were dissolved in 50 mL of deionized water, yielding solution A. The amalgamation was stirred for approximately 2 h. Concurrently, 1.5847 g of $(NH_4)_2HPO_4$ was introduced into 10 mL of deionized water and stirred for 20 min, resulting in solution B. Subsequently, solution B was slowly dripped into solution An under continuous stirring (~300 rpm) for 6 h. Following this, 1.5 mL of the resultant solution was injected into a 1 mol/L NaOH solution at a rate of 0.5 mL/s using a syringe equipped with a 23-gauge needle. Upon interaction with the NaOH solution, an immediate formation of gel fiber occurred. The gel fiber was immersed in the NaOH solution for 1 min, after which it was transferred to a mold and left undisturbed for 12 h. Subsequently, the scaffolds were rinsed with deionized water to eliminate excess NaOH and subjected to several rinses before being dried at 35 °C for 12 h. The dried scaffold were transferred into a muffle furnace (KSL-1400X-A3, Hefei Kejing Corp., China). The sintering protocol is illustrated in Fig. s1, typically, the temperature was raised to 800 °C at a rate of 4 °C/min under an air atmosphere and held for 2 h to remove organic substances from the scaffolds. Subsequently, the temperature was increased to 1200 °C at a rate of 2 °C/min, followed by a high-temperature hold for 3 h, after which the furnace was allowed to cool naturally to obtain the final scaffold product. The samples were labeled as 0.8Cu-HAp, 1.2Cu-HAp, and 1.6Cu-HAp to signify their respective Cu/Ca mole ratios of 0.8 %, 1.2 %, and 1.6 %, correspondingly.

2.2. Physicochemical characterization of the scaffold

The microstructure of the fabricated products underwent characterization employing field-emission scanning electron microscopy (SEM, VFGA3LMu, TESCAN, Czech). Fourier transform infrared spectroscopy (FTIR) using a Nicolet Magna 750 spectrometer (Nicolet Magna, USA) and X-ray powder diffraction (XRD) using an X'Pert PRO instrument (PANalytical Co., Netherlands) were employed to scrutinize the chemical composition and crystal structure of the products. Thermal analyses were conducted via Thermogravimetry–Differential Scanning Calorimetry (TG-DSC) using an STA 449 F5 apparatus (NETZSCH, Germany). The porous scaffold underwent three-dimensional imaging using a micro-computed tomography (micro-CT) scanner (Skyscan 1272, Bruker, Germany) with a scanning resolution set at 5 μm, and X-ray energy and current at 50 kV and 500 μA, respectively. Following the scan, images were reconstructed in 3D using the manufacturer's software, and the pore distribution within the sample was analyzed with Image-Pro Plus 6.0 software.

2.3. Ions releasing measurement of the scaffolds

To assess the ion release behavior of the scaffolds, concentrations of Ca^{2+} and Cu^{2+} ions were determined using inductively coupled plasma mass spectrometry (ICP-MS) with a PerkinElmer NexION 350 instrument (USA). The experimental setup involved immersing 42 mg of Cu-HAp scaffolds with varying Cu concentrations in 20 ml of 0.1 M Tris-HCl solution at pH 7.4. The mixtures were placed on a shaker table at a constant temperature of 35 °C. At specified time intervals, the mixtures were centrifuged, and 2 ml of supernatant samples were extracted for further analysis. An equivalent volume of fresh Tris-HCl solution was added to maintain the total solution volume. Measurements were conducted in triplicate for each time point to ensure accuracy and reliability of the data.

2.4. Cell culture

To explore the osteogenic potential of the scaffolds and assess the impact of copper release on cell growth and differentiation, mouse bone marrow mesenchymal stem cells (mBMSCs) and human umbilical vein endothelial cells (HUVECs) were used. mBMSCs were obtained from ATCC (USA) and cultured in high-glucose Dulbecco's minimal Eagle medium (DMEM) (Biological Industries, Israel) supplemented with 10 % fetal bovine serum and 1 % penicillin-streptomycin. HUVECs were cultured in low-glucose DMEM (Biological Industries, Israel) with

similar supplements and 1 % endothelial cell growth supplement. Both cell types were maintained at 37 °C in a humidified incubator with 5 % CO_2, with media refreshed every 2 days. When cultures reached 90–95 % confluence, cells were rinsed with PBS and detached using 0.25 wt% trypsin/EDTA solution (Gibco, USA). Detached cells were centrifuged at 1200 rpm for 5 min, collected, and prepared as a suspension for further experiments.

2.5. Cell viability, and proliferation affected by the scaffold and its releasing ions

mBMSCs were used to investigate cell viability on Cu-HAp scaffolds. Cells were seeded onto scaffolds in 48-well plates at a density of 1×10^5 cells per well. Proliferation was evaluated using the Cell Counting Kit-8 (CCK-8) assay (Dojindo, Japan) and live/dead staining (Yeasen BioTech, Shanghai, China). HUVECs were also seeded at the same density and proliferation assessed on days 1, 3, and 5. Following a 1-h incubation with CCK8 working solution, optical density (OD) was measured at 450 nm using a multimode microplate reader (Spark, TECAN, Switzerland). Samples were also stained with Calcein-AM/PI Double Staining working solution (YEASEN, China) and imaged using an inverted fluorescence microscope (DMi8, Leica, Germany).

To examine the impact of copper ions released from the Cu-HAp scaffold on cell proliferation, the scaffold was immersed in 5 ml of DMEM and gently shaken at 72 rpm. At specified time points, 2 ml of the extraction solution was taken, promptly replaced with an equal volume of fresh DMEM. The collected extraction solution, supplemented with fetal bovine serum and additional supplements, was then used to culture mBMSCs and HUVECs in 96-well plates at a seeding density of 8×10^3 cells/cm^2. Cell proliferation was assessed as previously described.

2.6. Alkaline phosphatase activity determination

mBMSCs were seeded at a density of 2×10^5 cells/well in 6-well plates. After attachment, the medium was replaced with osteogenic differentiation medium supplemented with 10 nM dexamethasone, 10 mM β-glycerophosphate, and 50 mM ascorbic acid, along with scaffold extracts. Cells were cultured for 7 days, washed with PBS, lysed, and the supernatant collected after centrifugation at 12,000 rpm for 15 min. Total protein content was determined using a BCA protein detection kit. Alkaline phosphatase (ALP) activity was measured using an ALP assay kit from Beyotime, China, in accordance with the manufacturer's instructions. The detailed procedure is as follows: After osteogenic induction, the culture medium was removed, and cells were lysed. Substrates and p-nitrophenol from the ALP assay kit were then added to the cell lysates, followed by incubation at 37 °C for 15 min. ALP activity was subsequently measured at an absorbance of 405 nm.

2.7. Alizarin Red S staining and quantitative analysis

To observe calcium nodule formation, mBMSCs were seeded at a density of 2×10^5 cells in a 6-well plate. After 24 h, fetal bovine serum and osteogenic factors were added to the scaffold extract, and this conditioned medium was co-cultured with the cells. The control group used osteogenic induction medium without the scaffold extract. After 14 days of co-culture, the cells were fixed with 4 % paraformaldehyde and stained with Alizarin Red solution, followed by washing with deionized water. The stained samples were photographed and imaged using an inverted microscope. For quantitative analysis, the stained cells were treated with 10 % hexadecylpyridinium chloride monohydrate, and the absorbance of the supernatant was measured at 562 nm.

2.8. Osteogenic and angiogenic gene expression

RT-PCR was used to evaluate gene expression. mBMSCs were seeded at 2×10^5 cells/well in 6-well plates and treated with osteogenic differentiation medium supplemented with scaffold extracts. RNA was harvested on days 7 and 14 using TRIzol reagent. HUVECs were seeded similarly and treated with scaffold extracts, with RNA harvested on days 4 and 7. cDNA was synthesized, and RT-PCR detected specific genes including COL-I, ALP, OC, OPN, Runx-2 for mBMSCs, and VEGF, bFGF for HUVECs. GAPDH and β-actin served as housekeeping genes. Gene expression was calculated using the $2^{-\Delta\Delta CT}$ method; the corresponding primers are shown in Table s1 and Table s2 (Supporting Information).

2.9. Western blot analysis

Western blotting assessed protein expression related to osteogenic and angiogenic properties. mBMSCs and HUVECs were cultured with osteogenic differentiation medium and scaffold extracts. Cells were lysed with RIPA buffer containing protease inhibitors, and protein extracts were separated by SDS-PAGE and transferred to PVDF membranes. Membranes were incubated with primary antibodies against RUNX2, OC, COL-I, VEGFA, and housekeeping proteins GAPDH and β-actin. Secondary antibodies were applied, and protein bands were visualized using ECL detection.

2.10. In vitro HUVECs migration and tube formation assay

To investigate the effect of scaffold extract on HUVEC migration, HUVECs were seeded in a 12-well plate, a scratch was made, and cells were treated with the growth medium containing the scaffold extract. The control group consisted of a normal growth medium without scaffold extract. Wound closure was quantified using ImageJ software. Tube formation was evaluated by seeding HUVECs with scaffold extract in Matrigel-coated wells. After 6 h, images were captured and analyzed using ImageJ software.

2.11. In vivo analysis of the scaffold

Animal studies were approved by the Animal Care and Experiment Committee of Gannan Medical University. To evaluate bone regeneration, a rat cranial defect model was employed. A full-thickness defect measuring 5 mm in diameter was surgically created on the side of each rat's skull. Scaffolds with different copper concentrations (0.8Cu-HAp, 1.2Cu-HAp, and 1.6Cu-HAp) were implanted into the defects. Each group included six samples for subsequent analysis. After 12 weeks post-surgery, the rats were euthanized, and the tissues were fixed for 24 h. The fixed samples were scanned using a micro-computed tomography scanner (Micro-CT, X-Cube, Molecubes, Ghent, Belgium), with an image resolution set to 20 μm. The scanning parameters included a voltage of 50 kV and a current of 400 μA, with each projection exposed for 50 ms. Three-dimensional reconstruction of the images was conducted using the vendor's software (Molecubes 1.7.6), followed by quantitative analysis of the 3D images using image analysis software (VivoQuant 5.1, Massachusetts, USA). The samples were then decalcified by immersion in a 20 % ethylenediaminetetraacetic acid (EDTA) solution for 18 days. Following decalcification, the samples were prepared for histological examination. Hematoxylin and eosin (H&E) staining and Masson's trichrome staining were performed on tissue sections according to standardized protocols provided by the manufacturer. To evaluate the angiogenic effect of the scaffold material, we performed immunohistochemical staining using a CD31 antibody (1:100, Servicebio Corp.). Tissue sections were prepared and stained, and results were observed under an optical microscope (ZEISS, Germany) to assess CD31 expression as an indicator of vascularization.

2.12. Statistical analysis

All data were presented as mean ± standard deviation (SD). Statistical analysis was conducted using one-way analysis of variance (ANOVA) followed by post-hoc Tukey's method for multiple

comparisons. The significance levels were indicated by asterisks, with *p < 0.05, **p < 0.01, ***p < 0.001, and ****p < 0.0001 considered statistically significant for all tests. GraphPad Prism 8.0.1 software (San Diego, USA) was employed for all statistical analyses.

3. Results and discussion

3.1. Characterization of Cu-HAp scaffolds

In this study, we successfully utilized a rapid gelation strategy to fabricate Cu-HAp porous scaffolds, as depicted in Scheme 1. Upon contact with the alkaline solution, the GG/HAp/Cu ions mixture system promptly gelled, forming continuous gel fibers. These gel fibers were then transferred into molds and subjected to drying and calcination processes, resulting in the final Cu-HAp porous scaffold. The size of the gel fibers was closely linked to the diameter of the injection needle. By employing different types of injection needles, gel fibers of varying diameters were produced (Fig. s2). Specifically, when using needle types 18, 22, and 27, the corresponding gel fiber sizes were 1 mm, 0.64 mm, and 0.38 mm, respectively, showcasing the adjustable nature of gel fiber diameter (Fig. 1a). Moreover, the gel fibers exhibited excellent flexibility and transferability. Even after repeated immersion in aqueous and alkaline solutions, the structural integrity of the gel fibers remained intact (Video S1), ensuring their potential for constructing complex structures. This potential was further demonstrated by 3D printing of GMU patterns featuring 3D grooves, as illustrated in Fig. 1b. By transferring the gel fibers into these grooves, we could directly fabricate complex-shaped 3D porous porous scaffolds. It is important to note that excessively large gel fiber diameters could hinder the fiber stacking process during molding, while overly small diameters might compromise the mechanical strength of the porous scaffold. Therefore, following careful screening and optimization, we selected a 23-gauge injection needle for subsequent experiments. Building upon this selection, we produced Cu-HAp scaffolds with three distinct copper doping concentrations (Fig. 1c). All three scaffold types exhibited porous characteristics, with SEM analysis revealing that the fibers were composed of stacked nanoparticles. Elemental mapping confirmed the homogeneous integration of Cu into the HAp structure, without any noticeable segregation phenomena (Fig. s3), The quantitative results obtained from Energy Dispersive X-ray Spectroscopy (EDS) analysis indicate that the final product of Cu/Ca (molar ratio) is slightly lower than the theoretical value. This discrepancy suggests that during the reaction process, some of the Cu formed other soluble or insoluble products instead of being fully incorporated into the crystal structure of HAp [19].

Supplementary data related to this article can be found online at https://doi.org/10.1016/j.mtbio.2024.101370

Afterwards, we delved into examining the impact of copper doping concentration on the physicochemical properties of Cu-HAp scaffolds. Fig. 2 illustrates our findings: The average pore sizes of 0.8Cu-HAp, 1.2Cu-HAp, and 1.6Cu-HAp scaffolds were 174.4 ± 13.7 μm, 166.7 ± 6.1 μm, and 171.7 ± 18.5 μm, respectively, indicating that variations in copper doping concentration did not significantly alter the pore size of the porous scaffold (Fig. 2a, b, 2c). Subsequently, we evaluated the thermal decomposition behavior of the three scaffolds through thermogravimetric analysis. The results revealed no significant difference in

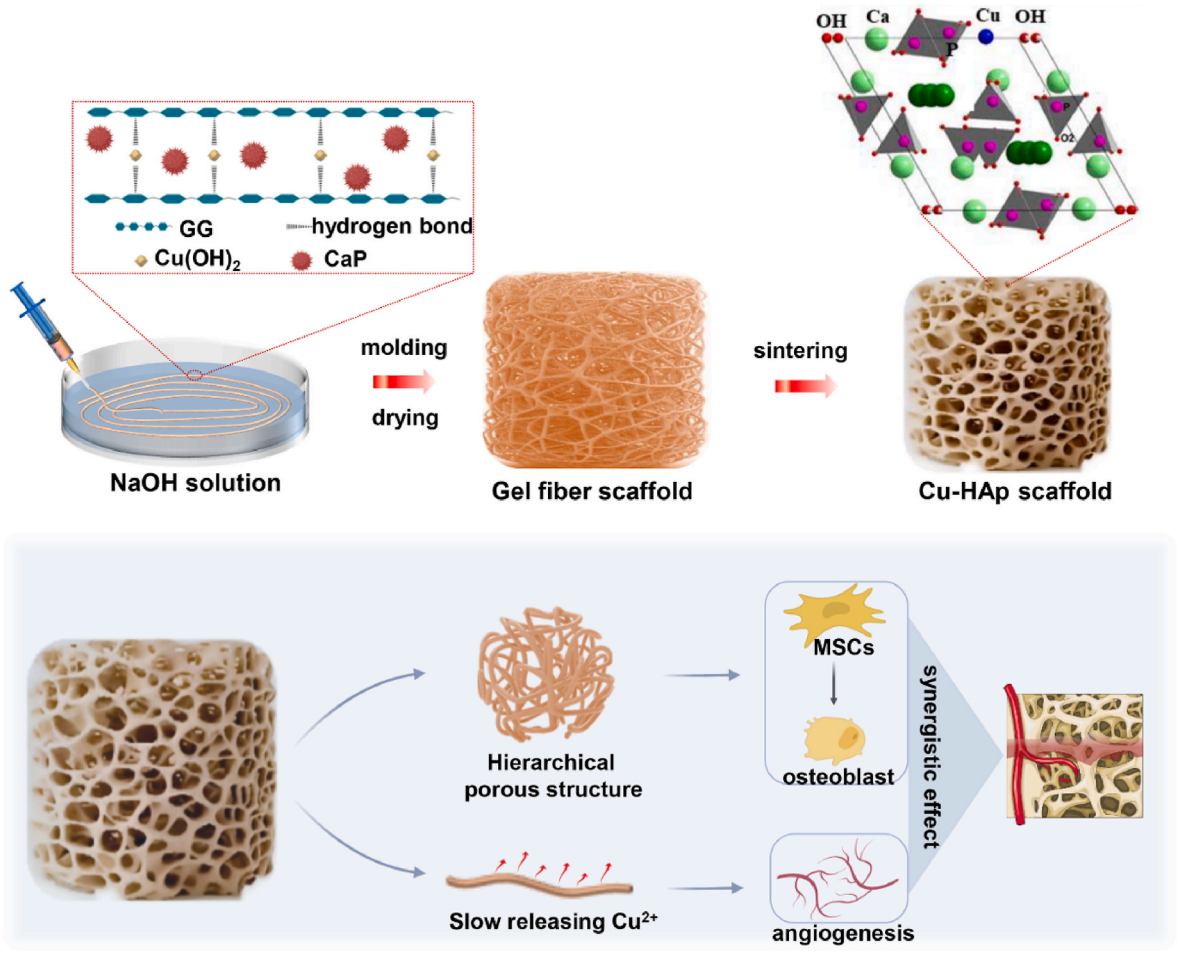

Scheme 1. Schematic illustration of a biomimetic hierarchical CuHAp porous scaffold for bone defect reconstruction.

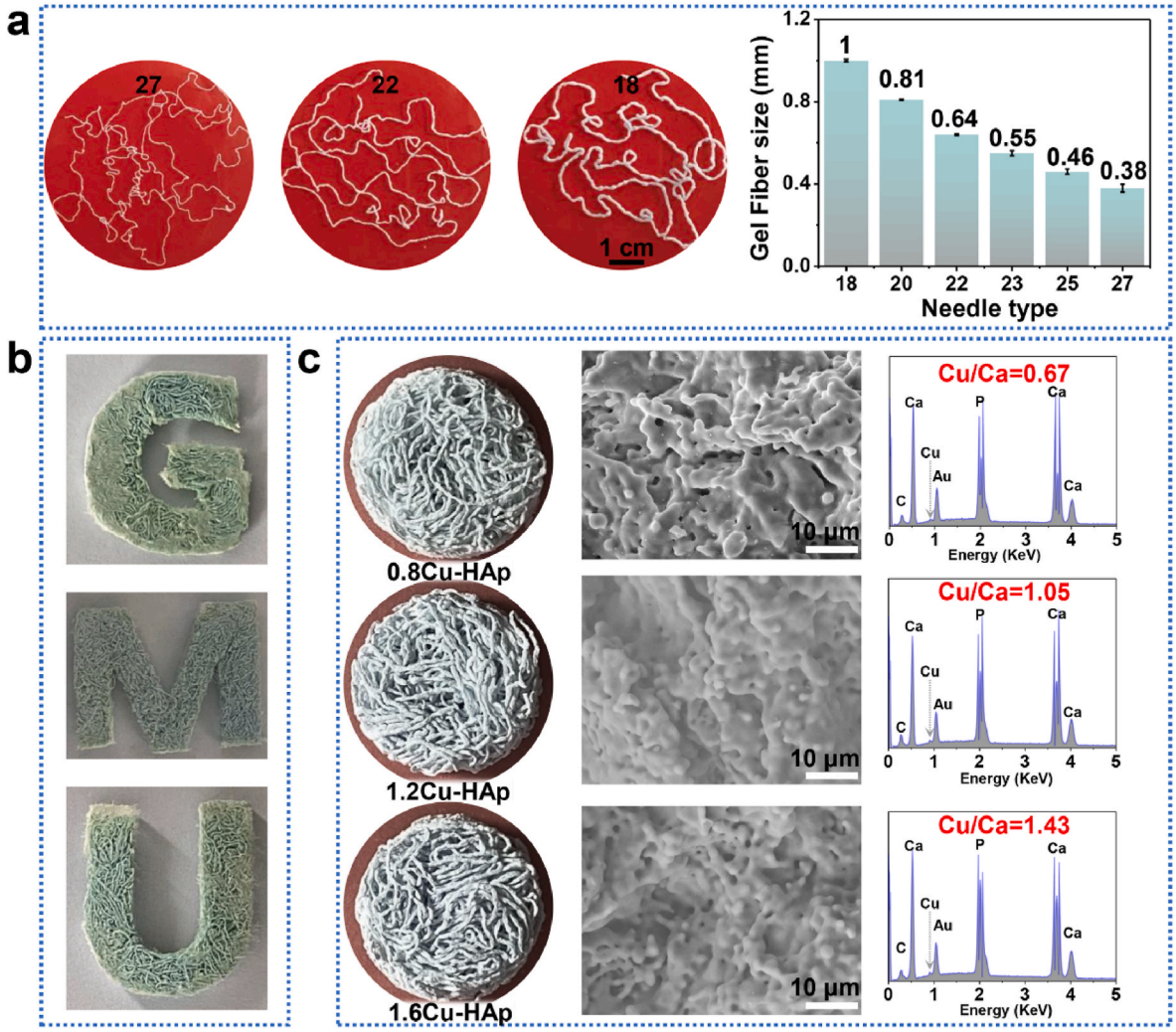

Fig. 1. (a) Optical Images of the gel fibers with different diameters and the corresponding relationship between fiber diameter and injection needle gauge; (b) Validation of the three-dimensional shaping performance of gel fibers; (c) Optical microscopy, SEM images, and energy-dispersive spectroscopy (EDS) quantitative analysis of Cu-HAp porous scaffolds.

mass loss during the low-temperature treatment stage (below 400 °C) among the three scaffolds. However, after sintering at 1200 °C, the weight loss of the 0.8Cu-HAp scaffold was lower than that of the other two groups, suggesting that excessive copper doping concentration could impact the stability of the HAp crystal structure [20] (Fig. 2d). Further examination showed that the porosity of the three scaffolds exhibited no significant difference (Fig. 2e), and their compressive strength slightly lower than the compressive strength of human cancellous bone (Fig. 2f) [21]. XRD results indicated that the XRD spectra of the three scaffold materials matched well with the standard PDF card of HAp, suggesting that the introduction of Cu ions into the HAp structure did not significantly affect the phase of the product (Fig. 2g). Subsequently, we explored the effect of copper doping concentration on the ion release behavior of the scaffold. Generally, the introduction of copper ions into the crystal structure of HAp would cause distortion of the HAp lattice structure and accelerate the dissolution of the HAp crystal, thereby increasing the rate of ion release. This conclusion was supported by the calcium ion release rate of the 0.8Cu-HAp scaffold being lower than that of the 1.2Cu-HAp and 1.6Cu-HAp groups (Fig. 2h). However, the copper ion release results revealed that the copper ion release rate of the 1.6Cu-HAp scaffold was the lowest, while conversely, the copper ion release rate of the 1.2Cu-HAp scaffold was the highest (Fig. 2i). Possible reasons for this phenomenon include: 1) The introduction of copper ions into the HAp structure exacerbates the dissolution behavior of the HAp crystal; 2) HAp and Cu ions exhibit strong affinity, with Cu ions tightly adsorbed on the surface of the HAp crystal in solution, and the stability of this adsorption is inversely correlated with the crystallinity of the HAp crystal [22]; 3) After Cu ions is introduced into the HAp crystal structure, the stability of the crystal structure weakens, leading to a decrease in crystal crystallinity, thereby enhancing the crystal's adsorption behavior to Cu ions in solution [23]. The combined effect of these factors results in the lower copper ion release behavior of the 1.6Cu-HAp scaffold. However, it is noteworthy that while the Cu ions concentration in the solution is low for the 1.6Cu-HAp scaffold, the surface of the crystal may still have a potential cytotoxic effect due to the enrichment of a large amount of Cu ions.

3.2. Cell viability, and proliferation affected by the scaffold and its releasing ions

The biocompatibility of the Cu-HAp scaffold was assessed using BMSCs and HUVECs as research models to examine cell activity on the scaffold surface. Following co-culturing with Cu-HAp scaffolds for 3 days, both BMSCs and HUVECs maintained high levels of activity, with no obvious dead cells observed in the field of view, suggesting that the introduction of copper ions into the HAp scaffold did not induce significant cytotoxicity (Fig. 3a and b). Subsequently, the proliferation

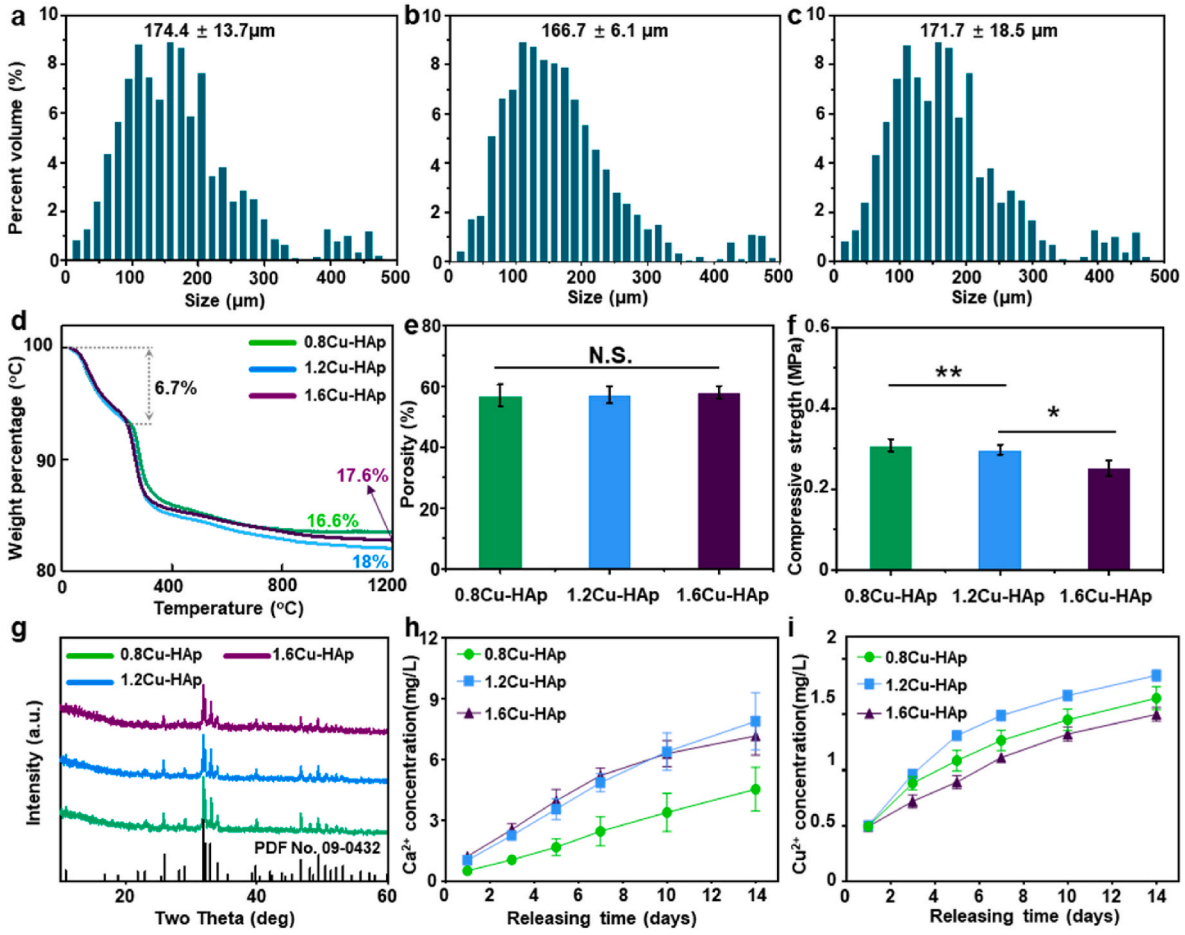

Fig. 2. Characterization of the physicochemical properties of Cu-HAp porous scaffolds. Pore size distribution of 0.8Cu-HAp (a), 1.2Cu-HAp (b), and1.6Cu-HAp (c); (d) TG curves of the Cu-HAp porous scaffold; porosity (e), compressive strength (f), XRD patterns (g), Ca^{2+} releasing behavior (h), and the Cu^{2+} releasing behavior (i) of the Cu-HAp porous scaffold.

behavior of cells on the Cu-HAp porous scaffold was investigated (Fig. 3c and d). The results indicated a negative correlation between the concentration of copper ion doping and the proliferation rate of cells. Specifically, the proliferation rate was highest on the surface of the 0.8Cu-HAp scaffold, while the 1.6Cu-HAp scaffold exhibited a significant inhibitory effect on cell proliferation (Fig. 3c). Moreover, compared to BMSCs, HUVECs displayed slightly weaker sensitivity to the copper ion content in the scaffold structure. Specifically, for BMSCs, the proliferation rate on the surface of the 1.2Cu-HAp scaffold was slower than that on the surface of the 0.8Cu-HAp scaffold, while for HUVECs, there was no significant difference in proliferation rate between the 0.8Cu-HAp and 1.2Cu-HAp scaffolds (Fig. 3d). This finding aligns with the results of Liu et al., who reported that the IC50 value of copper ions for HUVECs was 327.9 μM, three times that for BMSCs [24]. Furthermore, the effect of ion release from the scaffold on the proliferation behavior of BMSCs and HUVECs was investigated (Fig. 3e and f). The results indicated that ions released from the 1.6Cu-HAp scaffold significantly inhibited the proliferation of BMSCs (Fig. 3e), while there was no significant difference in proliferation rate on the surfaces of the other two groups of scaffolds. For HUVECs, there was no difference in proliferation on the surfaces of the 0.8Cu-HAp, 1.2Cu-HAp, and 1.6Cu-HAp scaffolds, further confirming the better tolerance of HUVECs to copper ions (Fig. 3f).

3.3. The osteogenic activity of Cu-HAp scaffolds and its ionic extracts

To assess the impact of Cu-HAp scaffolds on the osteogenic behavior of BMSCs, cells were co-cultured with scaffolds, and the expression of osteogenic genes and proteins in BMSCs was evaluated. After 7 days of co-culture, the 0.8Cu-HAp scaffold demonstrated higher OCN mRNA expression compared to the 1.6Cu-HAp scaffold group, while other osteogenic genes (OPN, ALP, and Runx2) exhibited no significant differences among the three groups (Fig. 4a). Extending the co-culture to 14 days still revealed no significant differences in the expression of other genes except for OCN. Further evaluation of early osteogenic factors (RUNX2 and COL I) and late osteogenic protein (OCN) secretion unveiled significant differences. After 7 days of co-culture, the 0.8Cu-HAp scaffold group showed significantly higher protein secretion levels of RUNX2 and ColI compared to the 1.6Cu-HAp scaffold group ($p < 0.05$). After 14 days, the OCN protein secretion level in the 0.8Cu-HAp scaffold group was significantly higher than that in the 1.2Cu-HAp and 1.6Cu-HAp scaffold groups ($p < 0.05$). The ALP activity of m-BMSCs on different Cu-HAp scaffolds also exhibited significant differences. The 0.8Cu-HAp scaffold group markedly enhanced ALP activity compared to the 1.2Cu-HAp and 1.6Cu-HAp scaffold groups ($p < 0.05$). Additionally, the ALP activity of the 1.2Cu-HAp scaffold group surpassed that of the 1.6Cu-HAp scaffold group ($p < 0.05$). These findings confirm the promotion of BMSCs osteogenesis by low-concentration copper-doped HAp scaffolds. Previous studies by Wu et al. and Dai et al. have also reported similar findings, demonstrating that the introduction of low concentrations of Cu ions into calcium phosphate/silicate enhances osteogenic gene expression and protein secretion, while higher concentrations lead to osteogenic inhibition effects [25,26].

Subsequently, a further investigation was conducted to ascertain the

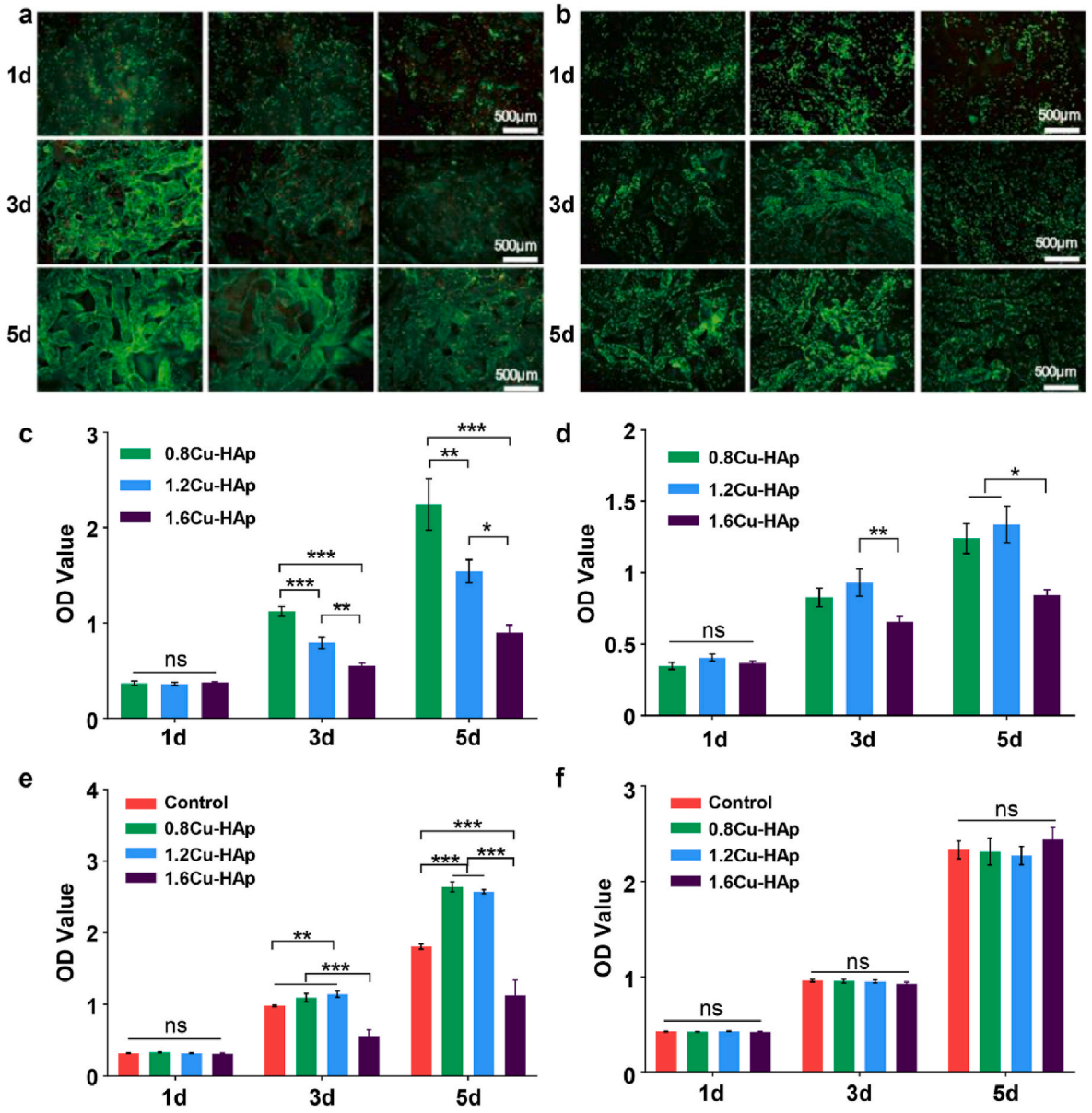

Fig. 3. The biocompatibility characterization of Cu-HAp scaffolds. (a) Live/dead staining of BMSCs cultured on the scaffold surface after 1 day, 3 days, and 5 days; (b) Live/dead staining of HUVECs cultured on the scaffold surface after 1 day, 3 days, and 5 days; (c) Proliferation of BMSCs on the surface of the scaffold; (d) Proliferation of HUVECs on the surface of the scaffold; (e) Effect of the ionic extracts from the scaffold on the proliferation behavior of BMSCs; (f) Effect of the ion extracts from the scaffold on the proliferation behavior of HUVECs.

potential influence of Cu-HAp scaffold extracts on the osteogenic behavior of mBMSCs. The mBMSCs were subjected to treatment with scaffold extract-conditioned medium. The results revealed that after 7 days of culture, the ion microenvironment provided by Cu-HAp scaffolds exhibited a certain degree of inhibitory effect on the osteogenic differentiation of mBMSCs, particularly evident in the suppression of the OCN gene. Notably, apart from the OCN gene, the ionic extract provided by the 0.8Cu-HAp scaffold showed no significant disparity in the expression levels of osteogenic marker genes such as OPN, ColI, ALP, and Runx2 compared to the control group. However, for the co-doped copper groups, namely the 1.2Cu-HAp and 1.6Cu-HAp scaffolds, their inhibitory effects on osteogenesis were significantly intensified compared to the control group (Fig. 5a). As the co-culture time prolonged, the inhibitory effects of the three scaffold groups on the osteogenic gene expression of mBMSCs gradually subsided, and the expression levels of some genes were marginally higher than those of the control group, indicating a progressive enhancement in the material's osteogenic activity (Fig. 5b). Studies have revealed that copper ions exhibit a certain inhibitory effect on the osteogenic differentiation of BMSCs, and this inhibitory effect is positively correlated with the concentration of copper ions [27]. Considering the ion release results (Fig. 2h and i), it was observed that the scaffolds rapidly released high concentrations of copper ions in the early stage, while with the extension of culture time, the scaffold surface underwent mineralization, leading to an increase in the specific surface area of the scaffold [28]. Additionally, the affinity between amorphous HAp and copper ions reduced the concentration of copper ions in the solution [29]. Consequently, the inhibitory effect of the co-culture late-conditioned medium on the osteogenic behavior of BMSCs gradually declined. Furthermore, an evaluation was conducted on the secretion status of osteogenic-related proteins, such as Runx2, ColI, and OCN, in mBMSCs stimulated by conditioned medium. The results indicated that the ionic extract provided by the 0.8Cu-HAp and 1.2Cu-HAp scaffolds promoted the secretion of both early osteogenic-related proteins (such as Runx2, ColI) and late osteogenic

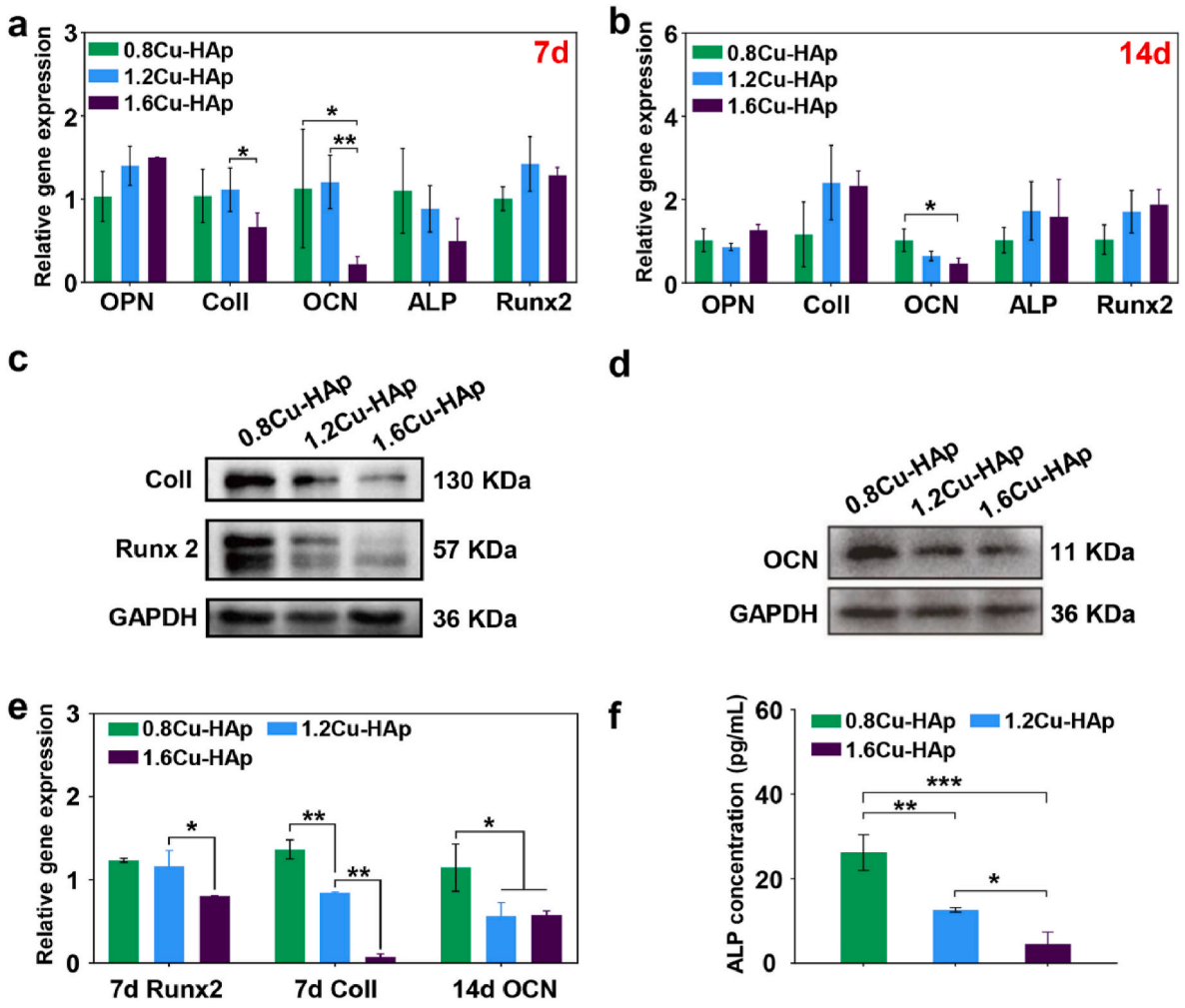

Fig. 4. Impact of Cu-HAp scaffolds on BMSCs osteogenic behavior. (a) Osteogenic gene expression after 7 days of co-culturing BMSCs with Cu-HAp scaffolds; (b) Osteogenic gene expression after 14 days of co-culturing BMSCs with Cu-HAp scaffolds; (c) Secretion levels of ColI and Runx2 proteins after 7 days of co-culturing BMSCs with Cu-HAp scaffolds; (d) Secretion levels of OCN protein after 14 days of co-culturing BMSCs with Cu-HAp scaffolds; (e) Quantitative analysis of ColI, Runx2, and OCN proteins; (f) ALP activity measurement after 7 days of co-culturing BMSCs with Cu-HAp scaffolds. *p < 0.05, **p < 0.01, ***p < 0.001.

marker protein (such as OCN) (Fig. 5c and d). Additionally, the protein quantification results further validated the aforementioned conclusions (Fig. 5e). Fig. 5f illustrates the effect of scaffold extract on m-BMSCs ALP activity, indicating that compared with the 1.2Cu-HAp and 1.6Cu-HAp extract groups, the 0.8Cu-HAp scaffold extract group exhibited the highest ALP activity, with no significant difference from the control group. Moreover, the ARS staining results further confirmed the high osteogenic activity of the 0.8Cu-HAp group (Fig. 5g and h). Generally, the expression trends of osteogenic genes and proteins should be consistent. However, within the cells, the transcriptional level and protein expression level are influenced by various factors, including the activity of transcription factors, post-transcriptional modifications, and protein stability, which may lead to inconsistencies between mRNA expression levels and protein expression levels [30]. Additionally, studies have shown that low-dose copper doping may promote the synthesis of osteogenic-related proteins, leading to an increase in their expression levels in cells. However, high-dose copper may lead to protein degradation or decreased stability, resulting in an inhibitory effect on protein expression levels [31]. Furthermore, Copper ions play a complex role in bone metabolism, and dysregulation of endogenous copper can lead to mesenkes disease, characterized by symptoms such as osteoporosis and bone fractures [32]. Research indicates that copper ions have a dual regulatory effect on osteogenesis. Some studies have shown that Cu ions can enhance the proliferation and osteogenic differentiation of mesenchymal stem cells [33], while others suggest that copper ions promote reactive oxygen species (ROS) accumulation, resulting in osteogenic inhibition [34].

This complexity is further evidenced by findings from Rodríguez et al., which indicate that copper ions can suppress ALP gene expression with minimal effect on its enzymatic activity, and simultaneously promote calcium nodule formation [35]. Typically, mRNA levels correlate with corresponding protein secretion; however, exceptions exist, as observed by Deng Hongwei's team, who found that mRNA expression does not always align with protein expression, particularly in biological regulatory processes [36].

While the osteogenic medium indeed enhances the osteogenic differentiation of BMSCs, our study emphasizes the role of the HAp scaffold in facilitating this process. Future investigations will explore the precise tuning of material structure and composition, as well as the potential of composite materials, to achieve efficient osteoinductive properties in both *in vitro* and *in vivo* settings without relying solely on osteogenic media.

3.4. The angiogenesis activity of Cu-HAp scaffolds and its ionic extracts

Vascularization stands as a pivotal stage in the process of bone repair [37]. Copper ions have been identified as playing a crucial role in angiogenesis [38]. Moreover, the sustained release behavior of copper

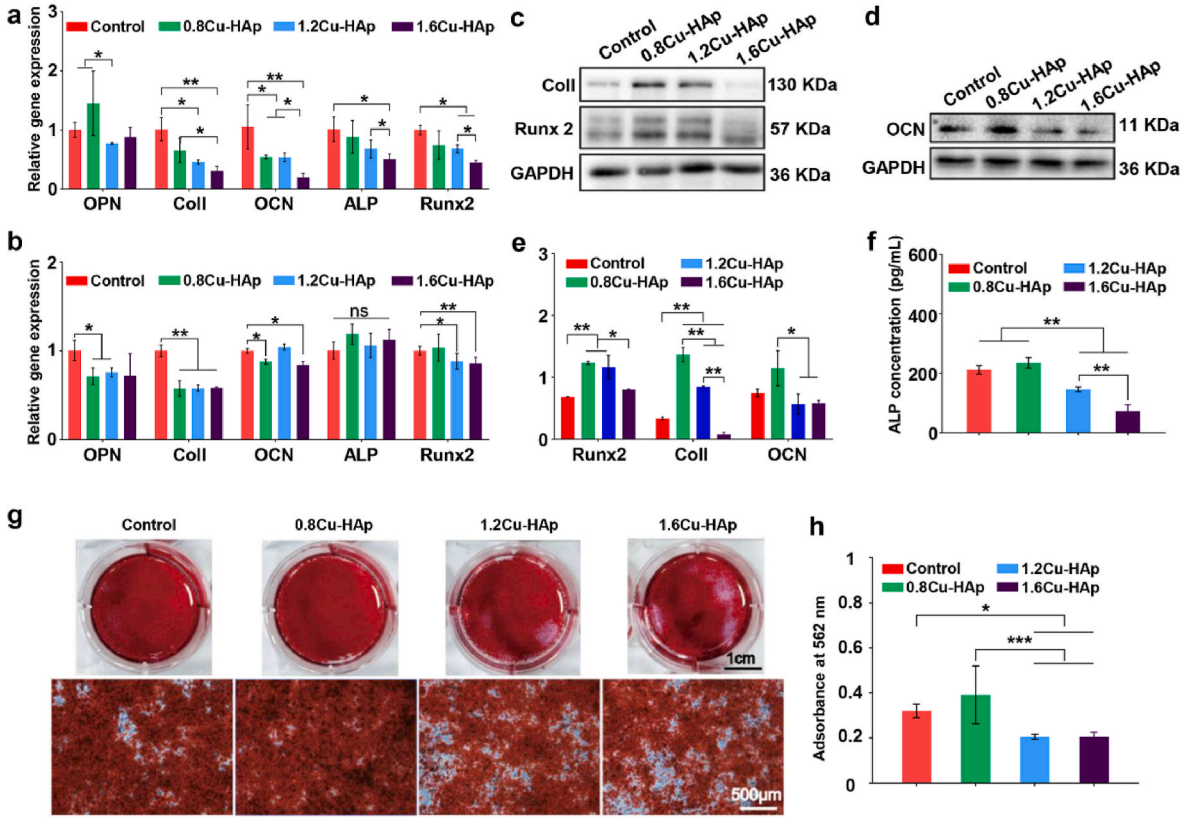

Fig. 5. Effects of Cu-HAp scaffold extracts on mBMSCs osteogenic behavior. (a) Osteogenic gene expression at (a) 7 days and (b) 14 days; (c) Col I and Runx2 protein expression at 7 days; (d) OCN protein expression at 14 days; (e) Quantitative measurement of the protein expression of Col I and Runx2 at 7 days, and OCN at 14 days; (f) ALP activity at 7 days; (g) Optical images and (h) quantitative analysis of ARS staining at 14 days.

ions within mineral scaffolds ensures continuous stimulation, thereby fostering *in vivo* angiogenesis [27]. Consequently, utilizing HUVECs as a model, we further explored the impact of Cu-HAp scaffolds and their ionic extracts on the vasculogenic behavior of these cells. Western blot analysis revealed that after four days of co-cultivation with the scaffolds, the protein expression levels of VEGF in HUVECs were higher on 0.8Cu-HAp and 1.2Cu-HAp scaffolds compared to the 1.6Cu-HAp group. Notably, there was no significant difference between the 0.8Cu-HAp and 1.2Cu-HAp scaffold groups, suggesting an inhibitory effect of the 1.6Cu-HAp scaffold on HUVECs' vasculogenic behavior. This inhibitory effect persisted with prolonged co-culture time (Fig. 6a). Combining these findings with the ion release results, we hypothesize that although the copper ion release rate from the 1.6Cu-HAp scaffold is lower than that of the other scaffold groups, the concentration of copper ions enriched on the scaffold surface may be higher, leading to a heightened cytotoxic response when cells are co-cultured with the scaffold.

Cell migration serves as a critical step in wound healing, with HUVECs capable of inducing rapid vascular formation at wound sites [39]. Hence, we employed a scratch assay to assess the effect of ionic extracts from the scaffold on HUVECs' migration behavior. As depicted in Fig. 6b, cell migration was evident in all groups, with the experimental groups exhibiting faster migration rates than the control group. Interestingly, there was no significant difference among the 0.8Cu-HAp, 1.2Cu-HAp, and 1.6Cu-HAp groups, which may be attributed to HUVECs' high tolerance to copper ion concentrations and the subtle differences in copper ion release concentrations among the three scaffold groups.

Furthermore, since the formation of tubular structures by endothelial cells constitutes another crucial parameter in functional vascularization [40], we evaluated the effect of the ionic extracts from scaffold on the tubular structure formation of HUVECs (Fig. 6c). The results indicated that the ionic extract from the 1.2Cu-HAp scaffold formed a greater number of well-defined capillary-like network structures, while the integrity of the network structures in the control and 1.6Cu-HAp groups were less satisfactory. Quantitative results corroborated these findings, with the ionic extract from the 1.2Cu-HAp group demonstrating the most robust promotion of vascularization, consistent with the ion release results (Fig. 2i). Additionally, RT-PCR results showed that during short-term co-culture, the ion scaffold extracts had no significant effect on the expression of angiogenesis-related genes (such as VEGF and bFGF) (Fig. 6d); however, with prolonged culture time, the ionic extract from the 1.6Cu-HAp group exhibited a promoting effect on VEGF and an inhibitory effect on bFGF gene expression (Fig. 6e).

Western blot analysis indicated a close correlation between ionic extract of the Cu-HAp scaffold and the secretion of the vascular marker VEGF in HUVECs. As illustrated in Fig. 6f, after four days of co-cultivation with conditioned medium, the 1.2Cu-HAp group exhibited the highest level of VEGF secretion. With continued co-culture time, the VEGF secretion level in the 1.2Cu-HAp group gradually declined, while that in the 0.8Cu-HAp group remained higher than that in the 1.2Cu-HAp and 1.6Cu-HAp groups.

In summary, incorporating an appropriate amount of copper ions into HAp scaffolds facilitates the migration, capillary network formation, and vasculogenic behavior of HUVECs. However, high-concentration copper doping may lead to significant cytotoxic reactions, characterized by sluggish cell migration, impeded capillary network formation, and reduced secretion levels of vascular marker proteins.

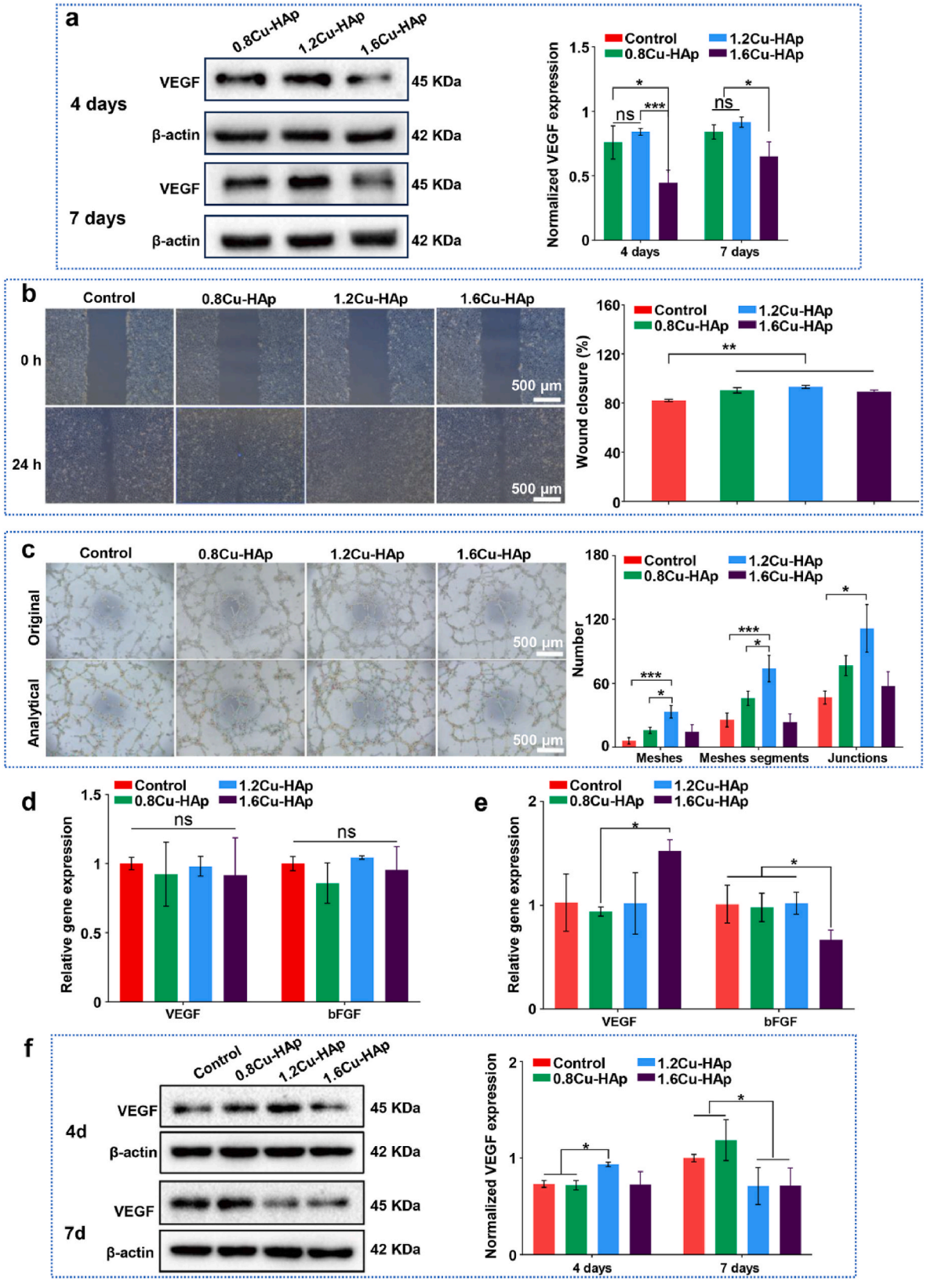

Fig. 6. The potential effect of Cu-HAp scaffolds and its ionic extract on the angiogenesis behavior of HUVECs. (a) immunoblotted image for VEGF and β-actin of HUVECs co-cultured with Cu-HAp scaffolds for 4 days and 7 days, and the corresponding relative quantitative mearsurement. Angiogenic potential of the scaffold extract: (b) Representative images of the scratch wound healing assay of HUVECs treated with conditioned medium and the quantitative analysis of the percentage of wound closure; (c) representative microscopy images of the tube formation of HUVECs after treated with the conditioned medium for 24 h and the quantitative assessment; RT-PCR analysis of angiogenesis-related gene expressions after 4 days (d) and (e) 7 days of treated with conditioned medium; (f) Immunoblotted images for VEGF and β-actin of HUVECs treated with conditioned medium for 4 days and 7 days, and the protein quantification (n = 3). *p < 0.05, **p < 0.01, ***p < 0.001.

3.5. *In vivo evaluation of osteogenic and angiogenic activities of Cu-HAp scaffolds*

In bone tissue engineering, the formation of new blood vessels and bone tissue are crucial indicators for evaluating the osteogenic activity of implant materials [4]. To validate the ability of the Cu-HAp scaffolds to promote bone tissue regeneration, a rat calvarial defect model was used for implantation experiments at 6 weeks and 12 weeks. The bone regeneration performance was analyzed through micro-CT and histological staining (Fig. 7).

As shown in Fig. 7a, after 6 weeks of implantation, new bone exhibited a growth pattern that crawled along the inner skull beneath the defect. Compared to the control group, all scaffold groups significantly promoted the regeneration of new bone tissue. However, there were still evident unrepaired defect gaps in the scaffold groups. After 12 weeks of implantation, the bone density of all Cu-HAp scaffolds and their integration with bone tissue significantly improved, indicating that Cu-HAp directly possesses excellent bone regeneration properties (Fig. 7b). Furthermore, the analysis of bone mineral density (BMD) (Fig. 7c) and bone volume percentage (BV/TV)(Fig. 7d) revealed that the amount of new bone formation increased with longer implantation times. The bone density and bone volume percentage in the 1.2Cu-HAp group were significantly higher than those in the control and 0.8Cu-HAp groups, suggesting that a moderate copper content optimally promotes bone formation [41].

Histological analysis using Hematoxylin and Eosin (H&E) staining at 6 and 12 weeks was conducted to evaluate bone tissue formation in Cu-HAp porous scaffolds. In the control group, no significant new bone formation was observed, primarily consisting of fibrous tissue. However, in the Cu-HAp scaffold groups, a small amount of new bone tissue was formed around the scaffolds. Notably, the 1.2Cu-HAp group exhibited the greatest thickness compared to other experimental and control groups, indicating that the 1.2Cu-HAp scaffold is more conducive to bone mineral deposition and new bone formation (Fig. s4). After 12

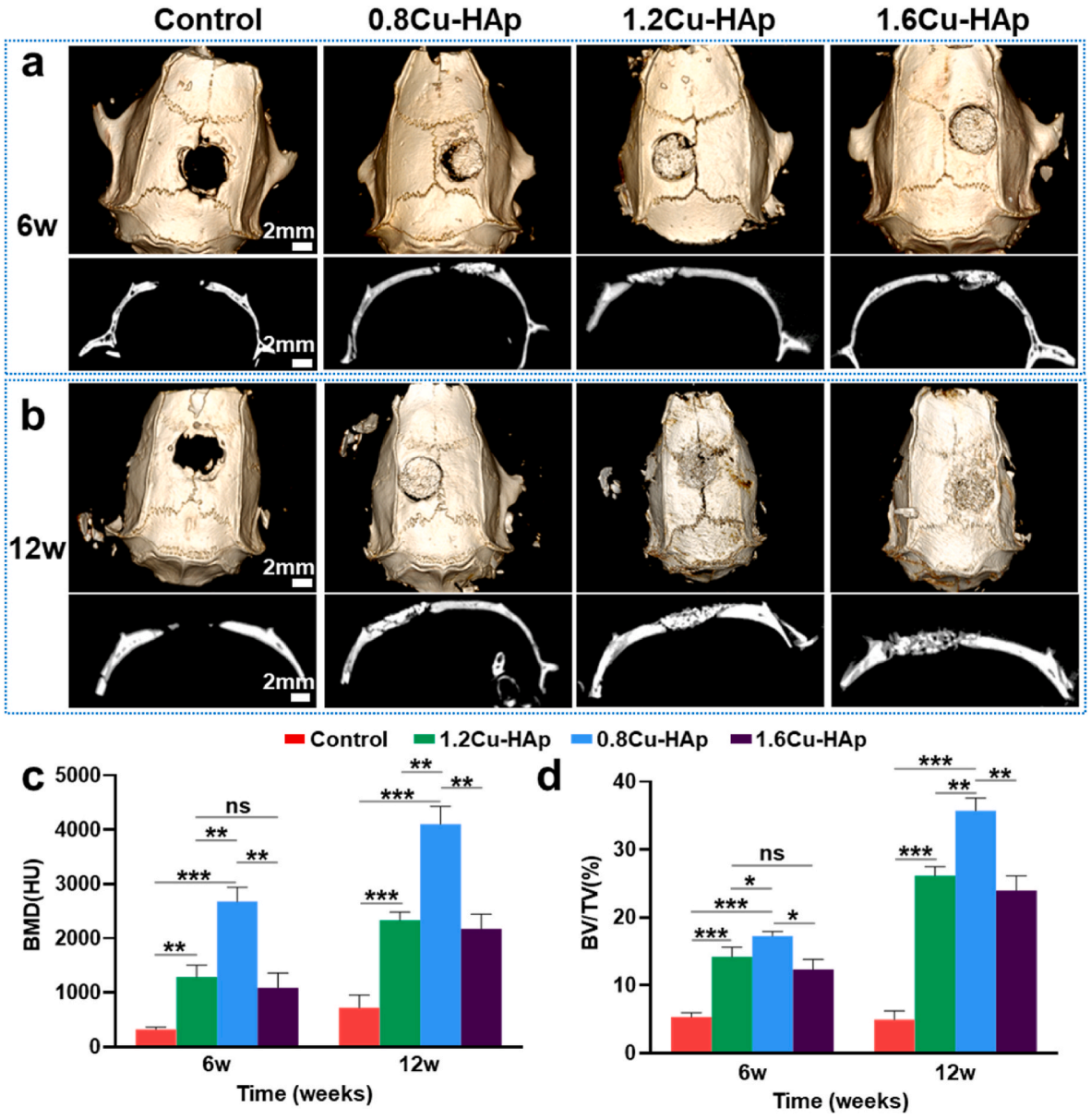

Fig. 7. The *in vivo* evaluation of bone regeneration ability of the Cu-HAp porous scaffolds in rat skull defect model. Representative micro-CT images in sagittal and cross-section view in different groups after transplation for 6 weeks (a) and 12 weeks (b). (c) Statistical analysis of the newly formed bone mineral density (BMD) for 6 weeks and 12 weeks (n = 3,*p < 0.05,**p < 0.01,***p < 0.001). (d) Quantitative statistical analyisis of the newly formed bone volume/total volume (BV/TV) for 6 weeks and 12 weeks.

weeks of implantation, the 1.2Cu-HAp group still maintained the highest thickness, suggesting that the long-term osteogenic activity of this material is relatively stable(Fig. 8a; Fig. s5 - s8). Additionally, clear new bone formation was observed at the interface between all Cu-HAp scaffolds and the bone, as well as at the bottom of the scaffolds, further confirming the characteristic of new bone crawling growth. Compared to the 0.8Cu-HAp and 1.6Cu-HAp groups, the new bone in the 1.2Cu-HAp scaffolds exhibited more ideal size and continuity (Fig. s7).

Masson staining was used to observe collagen fiber formation in different scaffold groups (Fig. 8b). At 6 weeks, the 1.2Cu-HAp group showed significantly more collagen fiber formation than the control and 0.8Cu-HAp groups, indicating good performance in early bone repair (Fig. s4). In addition to the observation of immature collagen matrix (blue) in the scaffold groups, a small amount of mature collagen matrix (red) was also distinctly observed. The mature collagen matrix was mainly distributed on the surface of the porous scaffold fibers, indicating that the scaffolds facilitate collagen deposition and maturation, that's consistent with previous published results [42]. After extending the implantation time to 12 weeks, the collagen fiber content in all Cu-HAp scaffolds further increased, with the collagen content in the 1.2Cu-HAp group being higher than that in the 0.8Cu-HAp and 1.6Cu-HAp groups (Fig. s9 – s12). Additionally, significant mature collagen matrix was observed in both the 1.2Cu-HAp and 1.6Cu-HAp groups (Fig. s11 and Fig. s12), further supporting the beneficial role of moderate copper content in bone repair.

CD31 staining assessed the vascularization in different groups. At 6 weeks post-implantation, compared to the control group, the 0.8Cu-HAp and 1.2Cu-HAp scaffold groups showed a significant acceleration in the vascularization process. However, for the 1.6Cu-HAp scaffold, the promotion of angiogenesis was weakened. Hence, copper doping at moderate concentrations (1.2Cu-HAp) may optimally enhance vascularization, as indicated by CD31 expression. However, at higher concentrations (1.6Cu-HAp), the effect may be detrimental, potentially due to cytotoxicity or other inhibitory effects of copper on endothelial cells. At 12 weeks post-implantation, the control group had the least vascularization, while the 1.2Cu-HAp showed significantly higher vascularization than the control, and 0.8Cu-HAp, with specific amounts at 1.2Cu-HAp: 7.27 % ± 0.603 per area, indicating that adequate copper content scaffolds effectively promote angiogenesis and thereby enhance bone tissue repair. For the 1.6Cu-HAp group, the vascular density within the scaffold significantly decreased compared to the 1.2Cu-HAp scaffold (Fig. 8c).

It has been reported that copper ions at moderate concentrations enhance the osteogenic differentiation of BMSCs [31,43], but also stimulate the expression of VEGF, which is essential for angiogenesis and subsequent bone repair [25,44]; furthermore, copper ions stimulate the

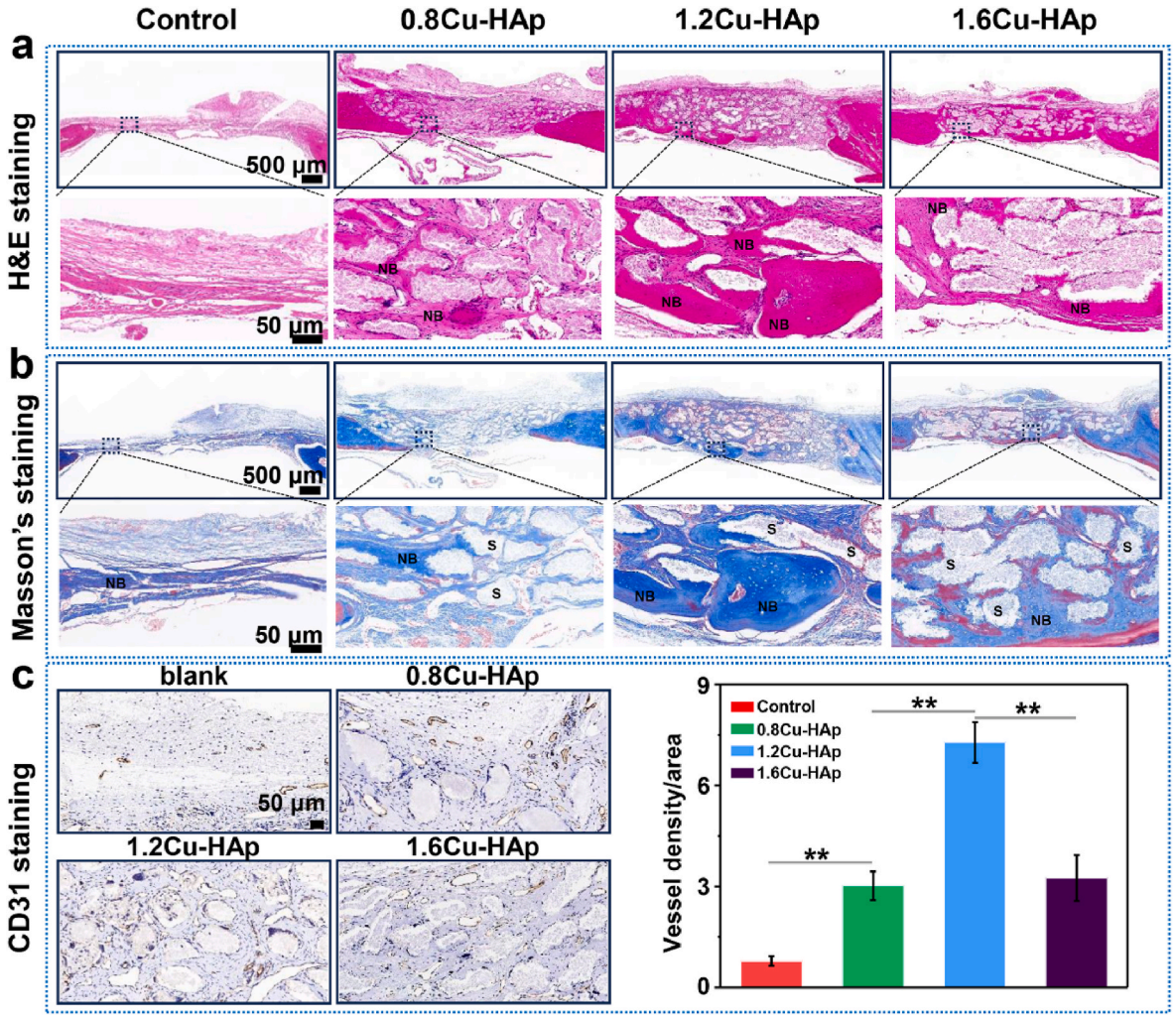

Fig. 8. The *in vivo* evaluation of bone regeneration ability of the Cu-HAp porous scaffolds through histological assays. (a) H&E staining of the regenerated bones induced by the Cu-HAp porous scaffolds after transplantation for 12 weeks (NB: new bone; S: scaffold); (b) Masson's trichrome staining of the regenerated bones induced by the Cu-HAp porous scaffolds after transplantation for 12 weeks (NB: new bone; S: scaffold). (c) At 12 weeks post-implantation, representative images of CD31 immunochemistry staining of different samples with quantification of the vessel density per area.

secretion of collagen and other bone matrix proteins by osteoblasts, promoting the formation of a robust protein matrix, and improving the structural integrity of the regenerated bone tissue [10,38]. Although numerous studies have demonstrated that Cu ions can promote angiogenesis by providing a hypoxic environment [45], the potential toxicity of Cu ions is an unavoidable factor [46]. This indicates that introducing an appropriate concentration of Cu ions into the scaffold is essential to balance its biocompatibility, osteogenic activity, and angiogenic activity.

These findings collectively demonstrate that Cu-HAp scaffolds, particularly those with 1.2 % copper content, significantly enhance both osteogenesis and angiogenesis, providing a promising strategy for bone tissue engineering applications.

In bone repair, the biomimetic construction of bone-like tissue and the establishment of a suitable osteogenic microenvironment are essential for accelerating the healing process. Trabecular bone features a complex hierarchical pore structure, where variations in pore size significantly impact cell adhesion, proliferation, osteogenic differentiation, vascular infiltration, and regeneration. By employing biomimetic principles, a porous structure resembling trabecular bone can be achieved through the disordered entanglement of individual fibers. However, challenges remain in the mass production of bone-like HAp ultralong fibers and in addressing their inherent brittleness. This study presents a rapid gelation strategy for fabricating HAp/guar gum composite fibers, effectively overcoming the scalability issues associated with HAp fiber production. These composite fibers demonstrate exceptional structural stability, flexibility, and transferability, accommodating personalized requirements for constructing hierarchical porous scaffolds that mimic bone. Importantly, the proposed construction strategy is straightforward and suitable for large-scale production, providing new insights for the development of porous scaffold systems utilizing other inorganic materials.

4. Conclusion

Here, leveraging the rapid gelation properties of the natural polysaccharide GG in specific environments, we have constructed ultra-long GG/HAp gel fibers. Utilizing these fibers as structural elements, we successfully developed HAp porous scaffolds with hierarchical pore structures. These scaffolds exhibit excellent features, including controllable fiber size, adjustable pore size, and tunable composition. *In vitro* experiments demonstrated that these scaffolds, when doped with low concentrations of copper, can promote the adhesion, proliferation, and osteogenic differentiation of bone marrow mesenchymal stem cells (BMSCs). Additionally, higher copper concentrations are more conducive to the expression of angiogenesis-related genes and proteins. A rat cranial defect model confirmed that the Cu-HAp scaffold exhibits superior bone regeneration performance. By rationally controlling the pore size distribution of the scaffold material and incorporating appropriate concentrations of copper doping to enhance chemical stimulation, the osteogenic and angiogenic activities of the HAp scaffold can be effectively improved, thereby promoting bone regeneration. This strategy may provide new insights for designing and optimizing novel calcium phosphate-based functional ceramic scaffolds, paving the way for more effective treatments in bone tissue engineering.

CRediT authorship contribution statement

Hui Yang: Writing – original draft, Data curation, Conceptualization. **Sirui Huang:** Data curation. **Xinwei Zhu:** Methodology. **Yasi Chen:** Methodology. **Chunming Xu:** Methodology. **Ruohan Li:** Methodology. **Pan Bu:** Methodology. **Yufan Jiang:** Methodology. **Changwei Li:** Methodology. **Jie Yang:** Methodology. **Zhenyi Chen:** Methodology. **Weijie Peng:** Writing – review & editing, Resources, Project administration. **Lin Liu:** Writing – original draft, Funding acquisition, Conceptualization.

Institutional Review Board statement

The protocol for the animal study was reviewed and approved by the Institutional Review Board of the Animal Ethics Committee at Gannan Medical University. (project identification code: NO. 2023231, 10 March 2023).

Declaration of competing interest

We declare that we have no financial and personal relationships with other people or organizations that can inappropriately influence our work, there is no professional or other personal interest of any nature or kind in any product, service and/or company that could be construed as influencing the position presented in, or the review of, the manuscript entitled.

Acknowledgments

This research was supported by National Natural Science Foundation of China (52462038); Natural Science Foundation of Jiangxi Province (20242BAB25357, GJJ2201422); Key Laboratory Program in Jiangxi Province (2024SSY06291); Scientific Research Foundation of Gannan Medical University (QD202145, QD202115, XN202004).

Appendix A. Supplementary data

Supplementary data to this article can be found online at https://doi.org/10.1016/j.mtbio.2024.101370.

Data availability

Data will be made available on request.

References

[1] A. Stahl, Y.P. Yang, Regenerative approaches for the treatment of large bone defects, Tissue Eng. B Rev. 27 (6) (2021) 539–547.
[2] A. Salhotra, H.N. Shah, B. Levi, M.T. Longaker, Mechanisms of bone development and repair, Nat. Rev. Mol. Cell Biol. 21 (11) (2020) 696–711.
[3] N.K. Karamanos, A.D. Theocharis, Z. Piperigkou, D. Manou, A. Passi, S.S. Skandalis, D.H. Vynios, V. Orian-Rousseau, S. Ricard-Blum, C.E. Schmelzer, A guide to the composition and functions of the extracellular matrix, FEBS J. 288 (24) (2021) 6850–6912.
[4] S. Stegen, N. Van Gastel, G. Carmeliet, Bringing new life to damaged bone: the importance of angiogenesis in bone repair and regeneration, Bone 70 (2015) 19–27.
[5] M. Bohner, L. Galea, N. Doebelin, Calcium phosphate bone graft substitutes: failures and hopes, J. Eur. Ceram. Soc. 32 (11) (2012) 2663–2671.
[6] L. Casarrubios, N. Gómez-Cerezo, S. Sánchez-Salcedo, M.J. Feito, M.C. Serrano, M. Saiz-Pardo, L. Ortega, D. de Pablo, I. Díaz-Güemes, B. Fernández-Tomé, S. Enciso, F.M. Sánchez-Margallo, M.T. Portolés, D. Arcos, M. Vallet-Regí, Silicon substituted hydroxyapatite/VEGF scaffolds stimulate bone regeneration in osteoporotic sheep, Acta Biomater. 101 (2020) 544–553.
[7] M. Fosca, J.V. Rau, V. Uskoković, Factors influencing the drug release from calcium phosphate cements, Bioact. Mater. 7 (2022) 341–363.
[8] M. Qu, X. Jiang, X. Zhou, C. Wang, Q. Wu, L. Ren, J. Zhu, S. Zhu, P. Tebon, W. Sun, Stimuli-responsive delivery of growth factors for tissue engineering, Adv. Healthcare Mater. 9 (7) (2020) 1901714.
[9] Z. Zhong, X. Wu, Y. Wang, M. Li, Y. Li, X. Liu, X. Zhang, Z. Lan, J. Wang, Y. Du, Zn/Sr dual ions-collagen co-assembly hydroxyapatite enhances bone regeneration through procedural osteo-immunomodulation and osteogenesis, Bioact. Mater. 10 (2022) 195–206.
[10] Y. Wang, W. Zhang, Q. Yao, Copper-based biomaterials for bone and cartilage tissue engineering, Journal of Orthopaedic Translation 29 (2021) 60–71.
[11] Y. Hui, Z. Dong, P. Wenkun, D. Yao, G. Huichang, L. Tongxiang, Facile synthesis of copper doping hierarchical hollow porous hydroxyapatite beads by rapid gelling strategy, Mater. Sci. Eng. C 109 (2020) 110531.
[12] L. Gibson, The mechanical behaviour of cancellous bone, J. Biomech. 18 (5) (1985) 317–328.
[13] G.L. Koons, M. Diba, A.G. Mikos, Materials design for bone-tissue engineering, Nat. Rev. Mater. 5 (8) (2020) 584–603.
[14] S. Kanwar, S. Vijayavenkataraman, Design of 3D printed scaffolds for bone tissue engineering: a review,, Bioprinting 24 (2021) e00167.

[15] Y. Liu, L. Cao, S. Zhang, L. Ji, J. Wang, C. Liu, Effect of hierarchical porous scaffold on osteoimmunomodulation and bone formation, Appl. Mater. Today 20 (2020) 100779.
[16] F. Chen, D. Porter, F. Vollrath, Morphology and structure of silkworm cocoons, Mater. Sci. Eng. C 32 (4) (2012) 772–778.
[17] F. Wu, S. Qiang, X. Zhang, F. Wang, X. Yin, L. Liu, J. Yu, Y.T. Liu, B. Ding, The rising of flexible and elastic ceramic fiber materials: fundamental concept, design principle, and toughening mechanism, Adv. Funct. Mater. 32 (45) (2022) 2207130.
[18] M. Alzweighi, R. Mansour, J. Lahti, U. Hirn, A. Kulachenko, The influence of structural variations on the constitutive response and strain variations in thin fibrous materials,, Acta Mater. 203 (2021) 116460.
[19] L. Thoraval, E. Thiébault, R. Siboni, A. Moniot, C. Guillaume, A. Jacobs, J.-M. Nedelec, G. Renaudin, S. Descamps, O. Valfort, The acute inflammatory response to copper (II)-doped biphasic calcium phosphates,, Materials Today Bio 23 (2023) 100814.
[20] Y.O. Nikitina, N. Petrakova, A. Ashmarin, D. Titov, S. Shevtsov, T. Penkina, E. Kuvshinova, S. Barinov, V. Komlev, N. Sergeeva, Preparation and properties of copper-substituted hydroxyapatite powders and ceramics, Inorg. Mater. 55 (2019) 1061–1067.
[21] P. Ammann, R. Rizzoli, Bone strength and its determinants, Osteoporosis international 14 (2003) 13–18.
[22] M. Šljivić, I. Smičiklas, I. Plećaš, M. Mitrić, The influence of equilibration conditions and hydroxyapatite physico-chemical properties onto retention of Cu2+ ions, Chem. Eng. J. 148 (1) (2009) 80–88.
[23] X. Liu, H. Yin, H. Liu, Y. Cai, X. Qi, Z. Dang, Multicomponent adsorption of heavy metals onto biogenic hydroxyapatite: surface functional groups and inorganic mineral facilitating stable adsorption of Pb (II), J. Hazard Mater. 443 (2023) 130167.
[24] K. Li, C. Xia, Y. Qiao, X. Liu, Dose-response relationships between copper and its biocompatibility/antibacterial activities, J. Trace Elem. Med. Biol. 55 (2019) 127–135.
[25] Z. Lin, Y. Cao, J. Zou, F. Zhu, Y. Gao, X. Zheng, H. Wang, T. Zhang, T. Wu, Improved osteogenesis and angiogenesis of a novel copper ions doped calcium phosphate cement, Mater. Sci. Eng. C 114 (2020) 111032.
[26] Q. Wu, S. Xu, X. Wang, B. Jia, Y. Han, Y. Zhuang, Y. Sun, Z. Sun, Y. Guo, H. Kou, Complementary and synergistic effects on osteogenic and angiogenic properties of copper-incorporated silicocarnotite bioceramic: in vitro and in vivo studies, Biomaterials 268 (2021) 120553.
[27] A. Jacobs, G. Renaudin, C. Forestier, J.-M. Nedelec, S. Descamps, Biological properties of copper-doped biomaterials for orthopedic applications: a review of antibacterial, angiogenic and osteogenic aspects, Acta Biomater. 117 (2020) 21–39.
[28] Y. Zhou, Z. Hu, W. Jin, H. Wu, M. Zuo, C. Shao, Y. Lan, Y. Shi, R. Tang, Z. Chen, Intrafibrillar mineralization and immunomodulatory for synergetic enhancement of bone regeneration via calcium phosphate nanocluster scaffold, Adv. Healthcare Mater. 12 (12) (2023) 2201548.
[29] Y. Liang, X. Jin, X. Xu, Y. Wu, A.A. Ghfar, S.S. Lam, C. Sonne, T.M. Aminabhavi, C. Xia, A novel porous lignocellulosic standing hierarchical hydroxyapatite for enhanced aqueous copper (II) removal,, Sci. Total Environ. 912 (2024) 168873.
[30] B. Schwanhäusser, D. Busse, N. Li, G. Dittmar, J. Schuchhardt, J. Wolf, W. Chen, M. Selbach, Global quantification of mammalian gene expression control, Nature 473 (7347) (2011) 337–342.
[31] M. Shi, Z. Chen, S. Farnaghi, T. Friis, X. Mao, Y. Xiao, C. Wu, Copper-doped mesoporous silica nanospheres, a promising immunomodulatory agent for inducing osteogenesis, Acta Biomater. 30 (2016) 334–344.
[32] Z. Zhang, H. Tang, T. Du, D. Yang, The impact of copper on bone metabolism,, Journal of Orthopaedic Translation 47 (2024) 125–131.
[33] X. Zhang, H. Liu, L. Li, C. Huang, X. Meng, J. Liu, X. Bai, L. Ren, X. Wang, K. Yang, L. Qin, Promoting osteointegration effect of Cu-alloyed titanium in ovariectomized rats, Regenerative Biomaterials 9 (2022).
[34] Y. Qi, H. Wang, X. Chen, Y. Zhu, The role of TGF-β1/Smad3 signaling pathway and oxidative stress in the inhibition of osteoblast mineralization by copper chloride,, Environ. Toxicol. Pharmacol. 84 (2021) 103613.
[35] J.P. Rodríguez, S. Ríos, M. Gonzalez, Modulation of the proliferation and differentiation of human mesenchymal stem cells by copper, J. Cell. Biochem. 85 (1) (2002) 92–100.
[36] Y. Guo, P. Xiao, S. Lei, F. Deng, G.G. Xiao, Y. Liu, X. Chen, L. Li, S. Wu, Y. Chen, H. Jiang, L. Tan, J. Xie, X. Zhu, S. Liang, H. Deng, How is mRNA expression predictive for protein expression? A correlation study on human circulating monocytes, Acta Biochimica et Biophysica Sinica 40 (5) (2008) 426–436.
[37] U. Saran, S.G. Piperni, S. Chatterjee, Role of angiogenesis in bone repair, Archieves of Biochemistry Biophysics 561 (2014) 109–117.
[38] C. Gérard, L.-J. Bordeleau, J. Barralet, C.J. Doillon, The stimulation of angiogenesis and collagen deposition by copper, Biomaterials 31 (5) (2010) 824–831.
[39] Y. Guan, H. Niu, Z. Liu, Y. Dang, J. Shen, M. Zayed, L. Ma, J. Guan, Sustained oxygenation accelerates diabetic wound healing by promoting epithelialization and angiogenesis and decreasing inflammation, Sci. Adv. 7 (35) (2021) eabj0153.
[40] I. Arnaoutova, H.K. Kleinman, In vitro angiogenesis: endothelial cell tube formation on gelled basement membrane extract, Nat. Protoc. 5 (4) (2010) 628–635.
[41] X. Qu, Z. He, H. Qiao, Z. Zhai, Z. Mao, Z. Yu, K. Dai, Serum copper levels are associated with bone mineral density and total fracture, Journal of orthopaedic translation 14 (2018) 34–44.
[42] W. Zhu, C. Li, M. Yao, X. Wang, J. Wang, W. Zhang, W. Chen, H. Lv, Advances in osseointegration of biomimetic mineralized collagen and inorganic metal elements of natural bone for bone repair, Regenerative Biomaterials 10 (2023) rbad030.
[43] I. Burghardt, F. Lüthen, C. Prinz, B. Kreikemeyer, C. Zietz, H.-G. Neumann, J. Rychly, A dual function of copper in designing regenerative implants,, Biomaterials 44 (2015) 36–44.
[44] A. Das, D. Ash, A.Y. Fouda, V. Sudhahar, Y.-M. Kim, Y. Hou, F.Z. Hudson, B. K. Stansfield, R.B. Caldwell, M. McMenamin, Cysteine oxidation of copper transporter CTR1 drives VEGFR2 signalling and angiogenesis, Nat. Cell Biol. 24 (1) (2022) 35–50.
[45] M. Wen, T. Wang, N. Li, Y. Wu, L. Zhang, Y. Xue, L. Shang, Polyphenol-copper derived self-cascade nanozyme hydrogel in boosting oxygenation and robust revascularization for tissue regeneration, Adv. Funct. Mater. (2024) 2403634.
[46] M.A. Kahlson, S.J. Dixon, Copper-induced cell death, Science 375 (6586) (2022) 1231–1232.